Journal of Materials Chemistry C

Effects of Polymer Crystallinity on Non-fullerene Acceptor based Organic Solar Cell Photostability

Journal:	*Journal of Materials Chemistry C*
Manuscript ID	TC-ART-08-2020-003969.R1
Article Type:	Paper
Date Submitted by the Author:	06-Oct-2020
Complete List of Authors:	Yi, Xueping; North Carolina State University Ho, Carr Hoi Yi; North Carolina State University, Department of Materials Science and Engineering Gautam, Bhoj; Fayetteville State University, Chemistry and Physics; North Carolina State University College of Sciences, Physics Lei, Lei; North Carolina State University, Department of Materials Science and Engineering Chowdhury, Ashraful Haider; South Dakota State University, Department of Electrical Engineering and Computer Science Bahrami, Behzad; South Dakota State University, Qiao, Qiquan; South Dakota State University, Department of Electrical Engineering and Computer Science So, Franky; North Carolina State University, Department of Materials Science and Engineering

Effects of Polymer Crystallinity on Non-fullerene Acceptor based Organic Solar Cell Photostability

*Xueping Yi[1], Carr Hoi Yi Ho[1], Bhoj Gautam[2], Lei Lei[1], Ashraful Haider Chowdhury[3], Behzad Bahram[3], Qiquan Qiao[3], and Franky So[1]**

[1] Department of Materials Science and Engineering, Organic and Carbon Electronics Lab (ORaCEL), North Carolina State University, Raleigh, NC 27695, United States
[2] Department of Chemistry, Physics and Materials Science, Fayetteville State University, Fayetteville, NC 28301, United States
[3] Department of Electrical Engineering, Center for Advanced Photovoltaics, South Dakota State University, Brookings, South Dakota 57007, United States

ABSTRACT: While there has been a rapid progress made in the performance of organic photovoltaic (OPV) cells in recent years, the device stability remains a major bottleneck for commercialization. In this work, we blended a stable acceptor (O-IDTBR) with two photostable donors (PTB7-Th and PffBT4T-2OD) having different polymer crystallinity, and the resulting devices show a significant difference in the OPV degradation rate. The OPV devices employing a highly crystalline polymer PffBT4T-2OD as an active layer show a good resistance against light soaking, maintaining 80% of the initial power conversion efficiency (PCE) up to 100 hours, while the devices employing an amorphous polymer PTB7-Th as an active layer show a significant PCE loss in the initial 20 hours mainly due to a rapid loss of the fill factor. By carrying out a comprehensive analysis of the device degradation mechanisms, we conclude that the origin for the PTB7-Th:O-IDTBR device degradation is the formation of mid-gap states under continuous sunlight illumination, leading to a significant drop in electron mobility. Device simulation revealed that deep traps act as charge recombination centers and increase the trap-assisted recombination rate, lowering the FF and J_{SC}.

Introduction:

In the last few years, significant progress has been made in small-molecule-acceptor based organic photovoltaic (OPV) cells, with power conversion efficiencies now extending to 18%[1,2], approaching to the requirements for commercialization. However, the OPV device lifetime still lags behind the device performance.[3,4]. To tackle this lifetime problem, researchers have been studying the fundamental degradation mechanisms in OPVs. The first order degradation of OPV cells comes from oxidation of low work function electrodes, and the degradation of the interface layers and photoactive layer.[5] While the degradation of the electrode and interface layers can be identified and addressed by utilizing different device architecture and encapsulation,[6,7] the details of the photoactive layer degradation of the photoactive layer are not well understood and the understanding of the degradation mechanisms is of the utmost importance.

Degradation of the photoactive layer mostly depends on materials photostability and the morphological stability of the blend.[7] The first requirements of a stable OPV photoactive layer are to have stable donor and acceptor materials against photo-oxidation.[8–10] For some materials photo-oxidation leads to changes in donor/acceptor materials, affecting their optical absorption properties.[10,11] However, a chemically stable donor and a stable acceptor alone do not necessarily result in a morphological stable active layer. The photoactive layer in an OPV cell is a bulk heterojunction (BHJ) consisting of a blend of an electron donating polymer and electron accepting molecules finely mixed at the nanoscale.[12–14] Besides the photochemical stability, the

morphological stability of the BHJ is also crucial for the device stability. In general, the molecular acceptors used in OPV are more mobile compared to the donor polymers, which may lead to stability issue.[15] Li et al. observed that the electroluminescence (EL) spectra of aged blends showed extra peaks attributed to pure PCBM emission, which is an indication for diffusion of PCBM.[16] Ghasemi et al. found that the high diffusivity of NF-SMA EH-IDTBR in blend is correlated with the severe degradation in the first few hours.[17] To inhibit the diffusion of small molecules acceptors, the choice of donor polymers is of vital importance. Durrant and et al.[18] reported that the photochemical stability of donor polymers is greatly affected by their crystallinity. In general, stable polymers are mostly crystalline exhibiting negligible oxygen quenching yields. McGehee et al.[19] reported that crystalline polymers may reduce the amount of mixed phase compared to the amorphous polymers, and reduce the device burn-in loss due to a decrease in nongeminate recombination.[20] Based on above studies, we hypothesize the crystallinity of donor polymer influences the degree of freedom for the small molecule acceptors such that it enhances the device stability.

It has been reported that due to the different polymer crystallinity, PTB7-Th and PffBT4T-2OD have very different BHJ morphology.[21–23] PTB7-Th is amorphous and its blend is characterized with two-phase model having the amorphous PTB7-Th-rich mixed domains and the acceptor-rich relatively pure domains, which has been studied in our previous work.[5,24] In contrast, PffBT4T-2OD[25] is well-known for its high crystallinity and could maintain its crystallinity to some extent after blending resulting in relative-pure donor and acceptor domains as well as some fraction of mixed

domains.[26,27] The different polymer crystallinity resulting in a different blend morphology allows us to study the impact of polymer crystallinity on device stability. To study the effects of polymer crystallinity on device stability, we blended a photo-stable NFA rhodanine-benzothiadiazole-coupled indacenodithiophene (O-IDTBR) [28] with two donor polymers having different crystallinity: poly[4,8-bis(5-(2-ethylhexyl)thiophen-2-yl)benzo][1,2-b;4,5-b']dithiophene-2,6-diyl-alt-(4-(2-ethylhexyl)-3-fluorothieno [3,4-b]thiophene-)-2-carboxylate-2-6-diyl) (PTB7-Th) which is an amorphous photoactive polymer and poly[(5,6-difluoro-2,1,3-benzothiadiazol-4,7-diyl)-*alt*-(3,3’’’-di(2-octyldodecyl)-2,2’;5’,2”;5”,2’’’-quaterthiophen-5,5-diyl) (PffBT4T-2OD) which is a highly crystalline polymer. In addition to crystallinity, these two polymers were chosen because they are chemically photostable under inert atmosphere, and their devices blending with O-IDTBR show a PCE higher than 8%. However, we found that when O-IDTBR is blended with the two donor polymers, there is a significant difference in the initial degradation rate of the resulting devices. Specifically, the highly-crystalline PffBT4T-2OD:O-IDTBR devices show a good resistance against light aging, maintaining 80% of the initial PCE up to 100 hours, while the PTB7-Th:O-IDTBR devices show a significant PCE loss of 30% during the initial 20 hours mainly due to the loss of FF. While we did not observe any significant differences in the film absorption spectra and exciton dissociation efficiencies, there is a decrease in electron mobility in the PTB7-Th blends due to light soaking. Furthermore, from the results of thermal admittance spectroscopy (TAS) measurements, we conclude that the formation of deep electron traps is the main cause

of the electron mobility loss under prolonged illumination. Device simulation based on the drift-diffusion model elucidates that an electron mobility value higher than 10^{-4} cm^2/Vs is needed to suppress trap-assistant recombination. Our results suggest the stable BHJ blend with a highly-crystalline polymer might be the main reason for its enhanced operation stability.

Results and Discussion:

To evaluate the device stability of the two blends, solar cells based on PTB7-Th:O-IDTBR and PffBT4T-2OD:O-IDTBR having a structure of ITO/ZnO/active layer/MoO_x/Ag were fabricated. As shown in **Figure S1** and **Table S1**, both PTB7-Th and PffBT4T-2OD exhibit a good PCE of 8% - 9%, making them good systems for the analysis of stability and the viability of NFA-based OPVs. **Figure 1** depicts the stability of the encapsulated devices under continuous 1 sun illumination in ambient condition with controlled device temperature at 30°C (**Figure S2**). It should be noted that our O-ITDBR based devices have a faster degradation rate than similar devices reported in the literature.[21,29] We believe that the faster degradation in our devices is due to the presence of UV light in the solar simulator we used in our measurements. Martorell et al. also showed that the presence of UV light leads to a rapid degradation of OPV cells.[30] Interestingly, both PTB7-Th:O-IDTBR and PffBT4T-2OD:O-IDTBR devices show an increase of Jsc in the first few hours as a result of the increasement of hole mobilities as shown in Figure 3(a), which will be discussed later. Overall, PffBT4T-2OD:O-IDTBR devices show a better photo-stability, with only 20% loss of PCE after 100 h of

light illumination. Notably, in these devices, FF is the only parameter that experiences a drop over 10%, while there is only a 5% decrease in J_{SC} and no change in V_{OC}. Similarly, FF accounts for the most loss in the PTB7-Th:O-IDTBR device, but the PCE shows a fast degradation in the first 20 h and levels off at a loss of ~40% (8% V_{oc}, 15% J_{sc}, and 25% FF loss). We have also conducted shelf-life measurements; for the devices stored in the dark under nitrogen, we found that both devices maintain >95% of its original PCE preserved after 2 days.

The distinct device photostability between PTB7-Th and PffBT4T-2OD when blending with the same acceptor O-IDTBR indicates that donor polymers play an important role in blend stability. The loss of photovoltaic properties can be due to either BHJ morphology changes or degradation at the interfaces. To eliminate the interfacial degradation possibility, we directly measured and compared the photocurrent generation from different BHJ layers using conductive atomic force microscopy (C-AFM) measurements, which simultaneously measure the topography and the electric current flow at the contact point of the tip with the film surface, offering insight into the charge generation properties by providing a high-resolution direct view of the local electrical properties of nanostructured polymer blends. **Figure S3** shows the topographical and current images of the polymer:O-IDTBR blend films, which were prepared under the same conditions as those used for device fabrication. For the PffBT4T-2OD blend films, the total currents from all pixels in the image were almost same before and after photo degradation, 711 pA and 702 pA respectively, which is consistent with the stable device properties. For the PTB7-Th blend films, the total

current was 870 pA as cast, and decreased to 288 pA after light illumination, suggesting the conductivity of PTB7-Th:O-IDTBR photo-aged films is degraded which might due to the stronger charge recombination. The C-AFM results confirm our hypothesis that the performance degradation we observed in **Figure 1** is due to the photoactive layer not the interface degradation.

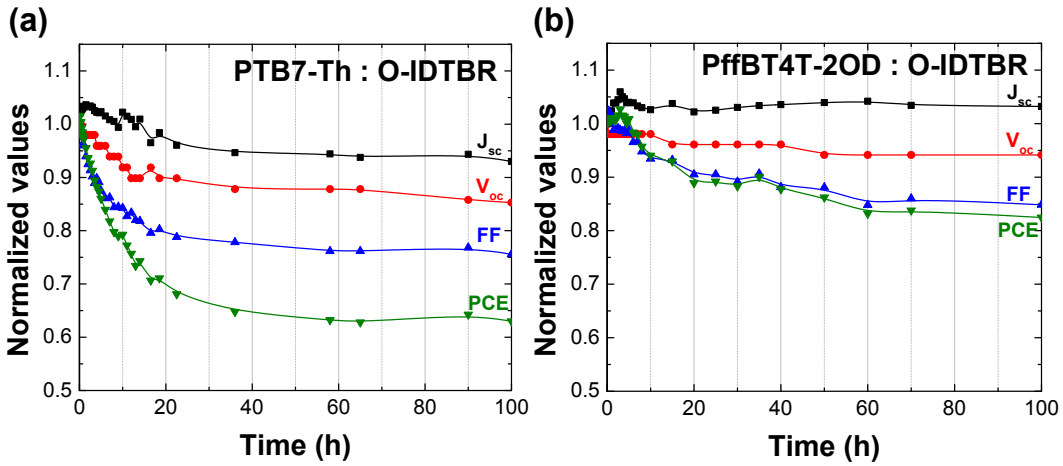

Figure 1. The device stability under continuous in a dry nitrogen atmosphere (a) PTB7-Th:O-IDTBR device parameters and (b) PffBT4T-2OD:O-IDTBR device parameters.

To understand the degradation mechanisms in the photo-aged non-fullerene based solar cells, we consider the following possible loss channels: light absorption, exciton dissociation and charge transport. First, we carried out ultraviolet-visible (UV-VIS) absorption to verify the film absorption stability under inert atmosphere. As the absorption spectral shape and intensity of UV-Vis absorption indicate local order of polymer chains in the films, any loss of order in the film due to photo-oxidation will be reflected in the absorption spectra.[11] Absorption spectra of pristine and blend samples aged under inert atmosphere are shown in **Figure S4**. All the films show no change up to 60 h of light illumination, indicating that blend film absorption is not affected by

light illumination under inert atmosphere. We then focus on the exciton dissociation dynamics at donor-acceptor interfaces by conducting femtosecond transient absorption spectroscopy (TA) on PTB7-Th:O-IDTBR and PffBT4T-2OD:O-IDTBR blends respectively. We measured the differential transmission of a broadband probe pulse after excitation of the sample with a 100 fs pump pulse tuned to 700 nm (1.8 eV), where both blend films have the maximum absorption. Same photoexcitation density was created in all thin films by tuning the pump fluence. The TA spectra at 10 ps delay between pump and probe pulses are shown in **Figure 2a and 2b** for PTB7-Th:O-IDTBR and PffBT4T-2OD:O-IDTBR fresh and light-aged blend films. The transient absorption spectra exhibit positive ground state bleaching (GSB) features[31] corresponding to film absorption peaks shown in **Figure S4** and the negative photo-induced (PIA) signal below 1.8 eV resulting from the excited-state absorption of charge transfer (CT) states.[32] It is noted that for both PTB7-Th and PffBT4T-2OD blends, there is no difference in GSB features before and after light degradation, whereas CT exciton signal of PffBT4T-2OD:O-IDTBR aged film is higher than its fresh sample which is an indication for stronger CT state population. This is very likely that the π-π interaction of PffBT4T-2OD becomes stronger as the polymers reorganize themselves at the donor-acceptor interfaces. The strong π-π makes CT exciton more delocalized and easier dissociated.[33]

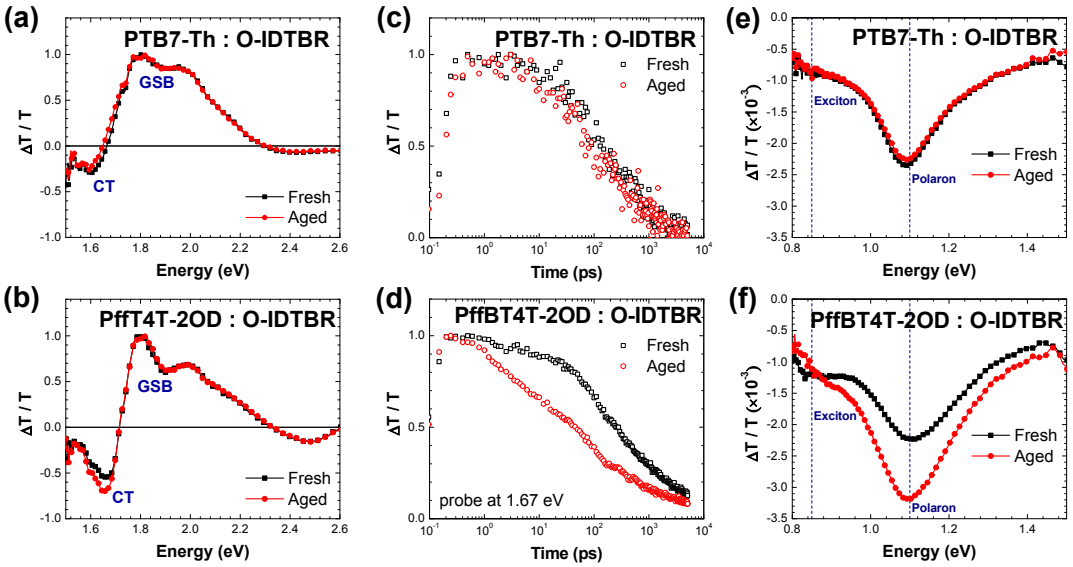

Figure 2. TA spectra at 10 ps for both (a) PTB7-Th:O-IDTBR and (b) PffBT4T-2OD:O-IDTBR fresh thin films and films under one sunlight illumination for 45 h. (c), (d)TA dynamics of CT excitons at 1.6 eV. (e), (f) TA spectra at 10 ps at NIR region. Signal at 0.85 eV is assigned to exciton and at 1.1 eV is assigned to polaron.

To compare the charge transfer exciton dynamics in the two blends, we monitored the evolution of the CT exciton features at ~1.6 eV as a function of time (**Figure 2c and 2d**), and found that the PTB7-Th blend CT exciton dynamic does not change with light illumination with a lifetime of ~ 30 ps. In contrast, the PffBT4T-2OD:O-IDTBR photo-aged film has a CT exciton lifetime ~ 5 ps, which is much shorter than that of fresh films (~ 60 ps). To determine the CT exciton lifetime of PffBT4T-2OD:O-IDTBR , we further studied polaron signals by measuring the transient absorption of probe pulses in the near-IR (NIR) region (0.8-1.5 eV) of the spectrum. **Figures 2e and 2f** show the NIR TA spectra at 10 ps delay between pump and probe pulses for the fresh and photo-aged samples. It is noted that the PffBT4T-2OD:O-IDTBR photo-aged sample shows a rise of polaron peak at 1.1 eV, which is correlated with the shorter CT exciton lifetime, indicating that the dissociation of CT excitons into polarons is more efficient in the

PffBT4T-2OD:O-IDTBR photo-aged film. This is consistent with the slight increase in Jsc in photo-aged PffBT4T-2OD:O-IDTBR devices. The unchanged PTB7-Th blend CT exciton dynamics and even more efficient exciton dissociation of the PffBT4T-2OD blend after illumination indicate that exciton dissociation cannot account for the device photodegradation observed in **Figure 1**.

Photoluminescence (PL) measurements were carried out to further confirm the exciton dissociation process in these devices, and the results are shown in **Figures S5**. PL quenching is a simple way to quantify the exciton dissociation efficiency by probing the direct charge transfer at the D-A interface. Here, we excited all blend films with or without light illumination, along with their pristine counterparts, and monitored their fluorescence emission. We found that both the PTB7-Th and PffBT4T-2OD films exhibit reasonably high PL quenching efficiencies of 97% and 91% respectively when blended with O-IDTBR. The PL quenching efficiencies almost do not change after blends exposed to light for 45 h, further confirming that exciton dissociation is not the root cause for poor PTB7-Th:O-IDTBR photostability.

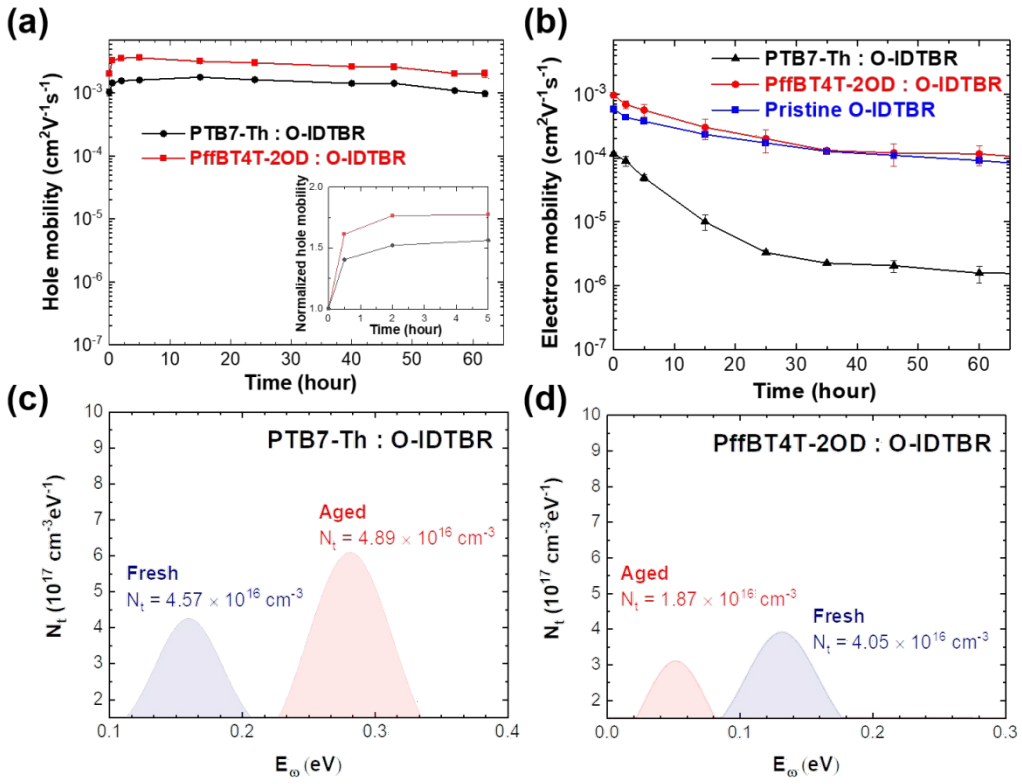

Figure 3. (a,b) Electron and hole mobility of the polymer:O-IDTBR blends and pristine O-IDTBR. The inset in (a) shows the normalized hole mobility changes in the first 5 hours. (c,d) Admittance spectroscopy showing trap Gaussian distribution in polymer:O-IDTBR fresh and aged films. E_ω is the trap energy level relative to the LUMO energy level.

In addition to charge generation, percolated charge transport pathways should be also stable under operation. To understand the influence of different morphology on charge transport and to find out the origin of the poor photo-stability in PTB7-Th:O-IDTBR cells, we measured the charge carrier mobility for holes and electrons individually in polymer:O-IDTBR blends using space-charge limited current model. **Figures 3a and 3b** show the time evolution of hole and electron mobilities for all blends under one-sun illumination. The hole mobility for all blends are stable, maintaining high values on the order of 10^{-3} cm^2/Vs under continuous light illumination up to 60 h, indicating efficient hole transport in both blend films. More importantly, we notice that the hole mobilities

of both PffBT4T-2OD:O-IDTBR and PTB7-Th:O-IDTBR actually increases in the first 5 hours, as shown in the inset of Figure 3(a), and this rise in hole mobility is consistent with the rise of Jsc in the same timescale. An increase in hole mobility enhances the hole transport, resulting in a rise in Jsc.[34] Different from the hole mobility, the electron mobility under light illumination shows a significantly different degradation trend: The PffBT4T-2OD:O-IDTBR electron mobility are relatively stable, which drops less than one order of magnitude, resembling the same trend as that in the pristine O-IDTBR devices, while the PTB7-Th:O-IDTBR electron mobility decreases by two orders of magnitude during the first 20 hours. The degradation trend of the electron mobility agrees well with that of device performance, showing the solar cell photodegradation is mainly caused by the electron mobility decrease. Moreover, we further conclude that the different electron mobility stability observed in two blends is due to the different polymer crystallinity as a high degree of polymer crystallinity could limit the degree of freedom for the small molecule acceptors.

Decreased charge carrier mobility has been explained due to charge traps by a slow dynamic process of trap charging and discharging.[9,11,35] Additionally, trap formation increases trap-assisted recombination, leading to the decrease in FF. The competition between charge recombination and extraction governs the device FF.[36] Further, deep trap states are known to pin the Fermi-level deep within the energy gap, potentially suppressing the achievable open circuit voltage.[37] To verify whether the electron mobility, Voc and FF decrease in the PTB7-Th:O-IDTBR devices is due to these trap states, we performance thermal admittance spectroscopy (TAS), which is used to

quantify mid-gap trap state energy and trap density by measuring the device capacitance versus frequency and temperature.[38] As only electron mobility decrease is observed in the single carrier devices, here, we assume the defects in the bandgap are mainly contributed by electron traps below LUMO level of BHJ blends with a Gaussian distribution. Charge transport usually proceeds via thermally activated hopping within localized sites. The detailed calculation is shown in Supporting Information. (**Figure S6 – Figure S7**) As shown in **Figure 3c and 3d,** both fresh PTB7-Th and PffBT4T-2OD blends have an electron defect band centered at ~ 150 meV below the LUMO level with a trap density of ~ 4×10^{16} cm^{-3}. However, after 50 h light illumination, the electron trap states of the PTB7-Th:O-IDTBR blend shift to a deeper energy level (240 meV) with a trap density of 5×10^{16} cm^{-3}, indicating deep electron traps were formed . Unlike the PTB7-Th blends, there is a decrease in the trap state energy level (from 145 meV to 50 meV) and trap density (from 4×10^{16} cm^{-3} to 2×10^{16} cm^{-3}) in the PffBT4T-2OD:O-IDTBR blend upon photo-aging. We should note that our admittance spectroscopy measurements only reflect the electron trap states in the bulk of the active layer. However, photo-degradation may also take place in the interlayers and interfaces. For example, light soaking of the ZnO ETL layer can lead to a reduced conductivity, resulting in a decrease in the apparent electron mobility measured in the PffBT4T-2OD:O-IDTBR single carrier devices. The relatively shallower trap states of PffBT4T-2OD:O-IDTBR facile electron transport in the active layer during photoaging, which leads to a stable FF and hence overall long operational device lifetime. This observation was expected as the PffBT4T-2OD polymer has better crystallinity than PTB7-Th, it

may limit the reorganization of the donor/acceptor domains into other thermodynamically stable orientations.[40]

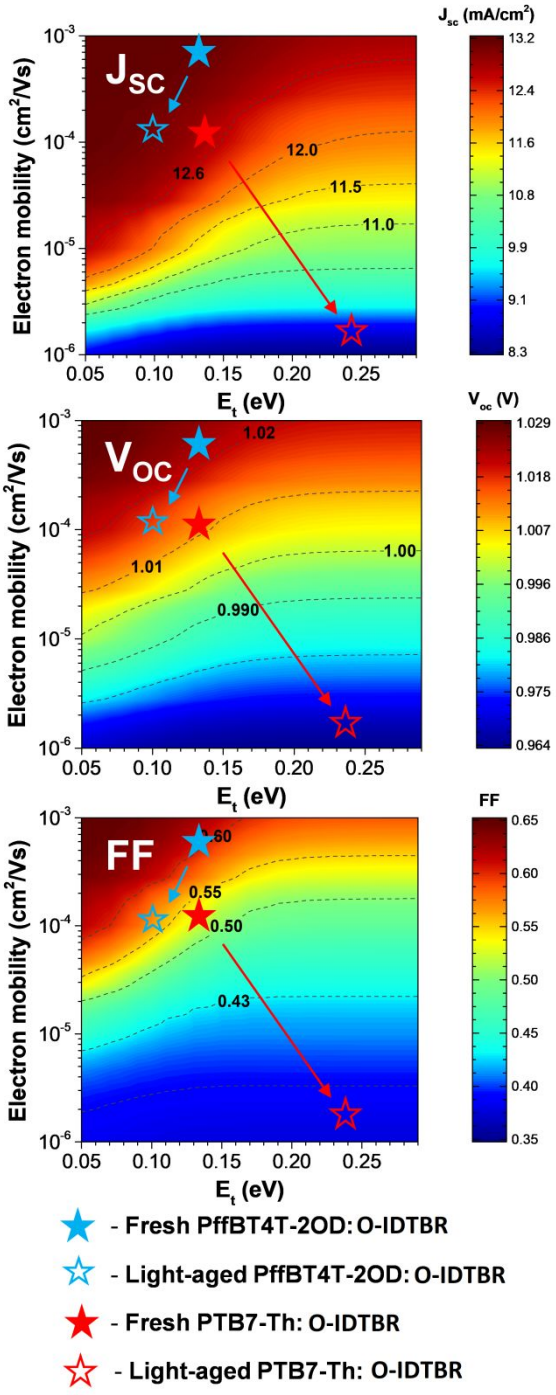

Figure 4. Device parameter prediction (plotted in color scale, with numbers on the

contour lines) for OPVs as a function of electron mobility (μ_e) and trap state energy level (E_t).

In order to verify the effect of electron mobility on the device performance, we used a device simulation tool – Setfos, which utilizes transfer matrix modeling to determine the layer specific absorbance in a device and numerically solves the drift-diffusion equations to simulate the device J–V curve under one-sun illumination.[41,42] In this simulation, we assume:

(1) bimolecular recombination process (Langevin recombination) is dominant and the rate of recombination (R) is described by the law of mass action, where k is the recombination rate constant (~10^{-12} cm^3 s^{-1}), n and p are electron and hole density, respectively, in solar cells.

$$R = knp$$

(2) Shockley–Read–Hall (SRH) recombination is also considered in the simulation to enable the trap-assisted recombination. We use a discrete level trap model with the trap density and its energy level values determined from the TAS results. Compared to the trap density which is all on the order of ~ 10^{16} cm^{-3}, the trap state energy shift is more pronounced. Therefore, we only vary the trap energy level in the simulation.

First, we simulate the fresh and aged PTB7-Th:O-IDTBR and PffBT4T-2OD:O-IDTBR device using the parameters from **Table S2,** and other fitting parameters are derived from the experimental J-V data. We find that the shape of the simulated J-V curves is in good agreement with the experimental J-V curves (**Figure S8**), validating that the simulator can reproduce the experimental device performance quite well using

values from the experimental results. Using the electron mobility (μ_e) and trap energy level (E_t) as the variable parameters, we examine how these two parameters will affect the OPV cell performance and what the requirements are to achieve high device stability. **Figure 4** displays the predicted device parameters FF, J_{sc} and V_{oc} for solar cells as a function of electron mobility and trap energy level. Overall, among the three parameters, FF shows the most sensitive dependence on μ_e and E_t. For comparison, V_{oc} decreases by 2% only when μ_e decreases by two orders of magnitude. Notably, the dependence of device parameters on electron mobility and trap state energy level can be divided into two trap-state-energy regions. When E_t < 150 meV, all device parameters can maintain the initially highest values with less than 5% decrease when $\mu_e > 10^{-4}$ cm^2/Vs and this is the case for the PffBT4T-2OD:O-IDTBR devices after photodegradation. When E_t is higher than 200 meV, the OPV device parameters are mainly determined by the electron mobility only. In the low-stability PTB7-Th:O-IDTBR devices as highlighted in the **Figure 4**, we see photo-aging decreases the electron mobility from 10^{-4} cm^2/Vs to 10^{-6} cm^2/Vs and increases the trap energy from 150 meV to 240 meV, significantly reducing the FF, because the trap-assisted recombination is strongly affected by the low charge-carrier mobility (**Figure S9**). In addition, the strong trap-assisted recombination increases the non-radiative open circuit voltage loss, resulting in Voc degradation.[43] These 2D simulation mappings are in good agreement with the device parameters from experimental device degradation measurements, and show that a high and stable electron mobility ($\mu_e > 10^{-4}$ cm^2/Vs) is the key parameter required to minimize the influence of charge traps and prevent trap-

assistant recombination when solar cells are operating under light. While we understand that light-induced defects and low electron mobility in O-IDTBR domains might lead to a loss in FF in the O-IDTBR-based devices, the question is the origin and chemical nature of these traps. To understand whether chemical changes in the bulk photoactive layer may explain the loss in FF, we carried out Fourier Transform Infrared (FTIR) measurements on fresh and photo-aged polymer:IDTBR films (**Figure S10**). Our results show that the FTIR profiles do not reveal any changes up to 60 hours of light exposure. In addition, the spectral shape and intensity of the UV-Vis absorption spectra of both blend films (**Figure S4**) do not change.[46] We therefore conclude that the different electronic trap formation is probably due to the different morphology in these two BHJ systems. High crystalline polymers might limit the degree of freedom for the small molecule acceptors such that they stabilize the BHJ, resulting in enhanced device stability.

Conclusion

In conclusion, we found that the polymer crystallinity is a key parameter determining the OPV device stability. Blending the same acceptor O-IDTBR with donors having different crystallinity results in different BHJ blend stability. The PffBT4T-2OD:O-IDTBR devices show a high stability under one-sun illumination, while PTB7-Th:O-IDTBR devices show a rapid PCE loss mainly due to the loss of FF. From the results of UV-Vis and transient absorption, we do not observe any difference between fresh

and light-aged samples in film absorption spectra and exciton dissociation efficiency. From thermal admittance spectroscopy, the poor photo-stability was found not only due to a significant electron mobility loss in the blend under continuous light illumination, but also a shift of trap states from a shallower level to the mid-gap level. Device simulation based on transfer matrix and drift-diffusion model suggests the formation of deep electron trap states from photodegradation of BHJ blend increases trap-assisted charge recombination, leading to a low FF and J_{SC}. The results suggest that the stability of the electron mobility is a key factor determining the device performance and highly crystalline donor polymers can inhibit the blend morphology change which might be a key aspect of its enhanced stability.

Experimental Section

Materials: PffBT4T-2OD, PTB7-Th, and O-IDTBR were purchased from1-Material.

Device Fabrication: The BHJ devices were fabricated with the inverted structure: glass/ITO/ZnO/Active layer/MoOx/Ag. Patterned ITO glass was precleaned in acetone and isopropanol. A thin layer of ZnO sol-gel was spin-coated (4000 rpm) onto the glass and baked at 150 °C for 30 min. For PffBT4T-2OD:O-IDTBR, the active layer solutions (13 mg/ml) of donor polymer: O-IDTBR (1:1) weight ratio were dissolved in chlorobenzene (CB). Both the solution and substrates were preheated at 100°C. Active layers were spin-coated at hot solution and hot substrates condition and at 1500 rpm to

get an active layer of ~ 90 nm. For PTB7-Th:O-IDTBR, the active layer solutions (20 mg/ml) of donor polymer: O-IDTBR (1:1) weight ratio were dissolved in chlorobenzene (CB). The substrates were then transferred into the evaporation chamber. Thermal evaporation was used for the deposition of 8 nm MoOx and 100 nm of Ag at a pressure of ~ 1×10^{-6} torr.

Device Characterization: J-V characteristics were acquired using a Keithley 4200 semiconductor parameter analyzer along with a Newport Thermal Oriel 94021 1000 W solar simulator, at 100 mW cm^{-2} incident power. EQE measurements were conducted using an in-house setup consisting of a Xenon DC arc lamp, an ORIEL 74125 monochromator, a Keithley 428 current amplifier, an SR 540 chopper system and an SR830 DSP lock-in amplifier from SRS. Films absorbance measurements were made with a Perkins Elmer UV–Vis spectrometer.

Transient Absorption Spectroscopy: Transient absorption data were collected using transient absorption spectroscopy setup. This setup consists of the spectrometer (Ultrafast Helios system) and amplified Ti:Saphhire Laser. The output of amplified Ti:Saphhire Laser provides 800 nm fundamental pulses at 1 kHz repetition rate which were split into two optical beams to generate pump and probe pulses. One fundamental beam was used to generate pump beam using an optical parametric amplifier (OPA) system (Coherent Opera Solo). A white light/NIR probe was generated by focusing another fundamental beam into a flint glass. Pump and probe beams were focused on a sample and probe light was collected by a charge-coupled device CCD device. The spectral detection region is 0.8 eV to 1.6 eV. The thin film samples were encapsulated

using UV curable clue before measurement. The instrument response function (IRF) was ~100 fs FWHM. The samples were excited with the excitation energy 2.68 eV for acceptor excitation and 1.75 eV for the donor excitation and the fractional change in transmission was detected in the probe range 0.8-1.6 eV at several time delays.

Thermal Admittance Spectroscopy: an AC signal of 20 mV is applied on organic solar cells to probe the capacitance at different frequencies. During the measurement, the samples are put in vacuum with temperature controlled by heater and liquid nitrogen.

Acknowledgements

This work was supported by the Office of Naval Research Grant N00014-17-1-2242 and N00014-17-1-2204.

References:

1 X. Xu, K. Feng, Z. Bi, W. Ma, G. Zhang and Q. Peng, *Adv. Mater.*, 2019, **0**, 0935–9648.

2 L. Meng, Y. Zhang, X. Wan, C. Li, X. Zhang, Y. Wang, X. Ke, Z. Xiao, L. Ding, R. Xia, H.-L. Yip, Y. Cao and Y. Chen, *Science*, 2018, **361**, 1094–1098.

3 N. Li, I. McCulloch and C. J. Brabec, *Energy Environ. Sci.*, 2018, **11**, 1355–1361.

4 S. A. Gevorgyan, N. Espinosa, L. Ciammaruchi, B. Roth, F. Livi, S. Tsopanidis, S. Züfle, S. Queirós, A. Gregori, G. A. dos R. Benatto, M. Corazza, M. V. Madsen, M. Hösel, M. J. Beliatis, T. T. Larsen-Olsen, F. Pastorelli, A. Castro, A. Mingorance, V. Lenzi, D. Fluhr, R. Roesch, M. Maria Duarte Ramos, A. Savva, H. Hoppe, L. S. A. Marques, I. Burgués, E. Georgiou, L. Serrano-Luján

and F. C. Krebs, *Adv. Energy Mater.*, 2016, **6**, 1–9.

5 Y. Zhu, A. Gadisa, Z. Peng, M. Ghasemi, L. Ye, Z. Xu, S. Zhao and H. Ade, *Adv. Energy Mater.*, 2019, **9**, 1–13.

6 N. Y. Doumon, M. V. Dryzhov, F. V. Houard, V. M. Le Corre, A. Rahimi Chatri, P. Christodoulis and L. J. A. Koster, *ACS Appl. Mater. Interfaces*, 2019, **11**, 8310–8318.

7 Z. Li, E. Speller, J. Durrant, J.-S. Kim, W. Tsoi, A. J. Clarke, J. Luke, T. Wang, H. C. Wong, H. Lee and N. Li, *J. Mater. Chem. A*, , DOI:10.1039/c9ta05235f.

8 N. Y. Doumon and L. J. A. Koster, *Sol. RRL*, 2019, **3**, 1800301.

9 Y. Wang, M. J. Jafari, N. Wang, D. Qian, F. Zhang, T. Ederth, E. Moons, J. Wang, O. Inganäs, W. Huang and F. Gao, *J. Mater. Chem. A*, 2018, **6**, 11884–11889.

10 H. S. Silva, I. F. Domínguez, A. Perthué, P. D. Topham, P. O. Bussière, R. C. Hiorns, C. Lombard, A. Rivaton, D. Bégué and B. Pépin-Donat, *J. Mater. Chem. A*, 2016, **4**, 15647–15654.

11 M. O. Reese, A. M. Nardes, B. L. Rupert, R. E. Larsen, D. C. Olson, M. T. Lloyd, S. E. Shaheen, D. S. Ginley, G. Rumbles and N. Kopidakis, *Adv. Funct. Mater.*, 2010, **20**, 3476–3483.

12 G. Yu, J. Gao, J. C. Hummelen, F. Wudl and A. J. Heeger, *Science (80-.).*, 1995, **270**, 1789–1791.

13 A. J. Heeger, *Adv. Mater.*, 2014, **26**, 10–28.

14 G. Dennler, M. C. Scharber and C. J. Brabec, *Adv. Mater.*, 2009, **21**, 1323–1338.

15 N. D. Treat, M. A. Brady, G. Smith, M. F. Toney, E. J. Kramer, C. J. Hawker and M. L. Chabinyc, *Adv. Energy Mater.*, 2011, **1**, 82–89.

16 N. Li, J. D. Perea, T. Kassar, M. Richter, T. Heumueller, G. J. Matt, Y. Hou, N. S. Güldal, H. Chen, S. Chen, S. Langner, M. Berlinghof, T. Unruh and C. J. Brabec, *Nat. Commun.*, , DOI:10.1038/ncomms14541.

17 M. Ghasemi, H. Hu, Z. Peng, J. J. Rech, I. Angunawela, J. H. Carpenter, S. J. Stuard, A. Wadsworth, I. McCulloch, W. You and H. Ade, *Joule*, 2019, **3**, 1328–1348.

18 Y. W. Soon, S. Shoaee, R. S. Ashraf, H. Bronstein, B. C. Schroeder, W. Zhang, Z. Fei, M. Heeney, I. McCulloch and J. R. Durrant, *Adv. Funct. Mater.*, 2014, **24**, 1474–1482.

19 T. Heumueller, W. R. Mateker, I. T. Sachs-quintana, K. Vandewal, J. A. Bartelt, T. M. Burke, T. Ameri, J. Brabec and M. D. Mcgehee, 2014, 2974–2980.

20 R. Xue, J. Zhang, Y. Li and Y. Li, *Small*, 2018, **14**, 1–24.

21 H. Cha, J. Wu, A. Wadsworth, J. Nagitta, S. Limbu, S. Pont, Z. Li, J. Searle, M. F. Wyatt, D. Baran, J. S. Kim, I. McCulloch and J. R. Durrant, *Adv. Mater.*, 2017, **29**, 1–8.

22 H. Cha, S. Wheeler, S. Holliday, S. D. Dimitrov, A. Wadsworth, H. H. Lee, D. Baran, I. McCulloch and J. R. Durrant, *Adv. Funct. Mater.*, 2018, **28**, 1–11.

23 W. Li, M. Chen, J. Cai, E. L. K. Spooner, H. Zhang, R. S. Gurney, D. Liu, Z. Xiao, D. G. Lidzey, L. Ding and T. Wang, *Joule*, 2019, **3**, 819–833.

24 X. Yi, B. Gautam, I. Constantinou, Y. Cheng, Z. Peng, E. Klump, X. Ba, C. H.

Y. Ho, C. Dong, S. R. Marder, J. R. Reynolds, S. W. Tsang, H. Ade and F. So, *Adv. Funct. Mater.*, , DOI:10.1002/adfm.201802702.

25 Y. Liu, J. Zhao, Z. Li, C. Mu, W. Ma, H. Hu, K. Jiang, H. Lin, H. Ade and H. Yan, *Nat. Commun.*, 2014, **5:5293**, doi: 10.1038/ncomms6293.

26 D. Baran, T. Kirchartz, S. Wheeler, S. Dimitrov, M. Abdelsamie, J. Gorman, R. Ashraf, S. Holliday, A. Wadsworth, N. Gasparini, P. Kaienburg, H. Yan, A. Amassian, C. J. Brabec, J. Durrant and I. McCulloch, *Energy Environ. Sci.*, 2016, **9**, 3783–3793.

27 H. Hu, P. C. Y. Chow, G. Zhang, T. Ma, J. Liu, G. Yang and H. Yan, *Acc. Chem. Res.*, 2017, **50**, 2519–2528.

28 J. Luke, E. M. Speller, A. Wadsworth, M. F. Wyatt, S. Dimitrov, H. K. H. Lee, Z. Li, W. C. Tsoi, I. McCulloch, D. Bagnis, J. R. Durrant and J. S. Kim, *Adv. Energy Mater.*, 2019, **9**, 1–14.

29 N. Gasparini, M. Salvador, S. Strohm, T. Heumueller, I. Levchuk, A. Wadsworth, J. H. Bannock, J. C. de Mello, H. J. Egelhaaf, D. Baran, I. McCulloch and C. J. Brabec, *Adv. Energy Mater.*, 2017, **7**, 1–7.

30 C. J. Schaffer, C. M. Palumbiny, M. A. Niedermeier, C. Burger, G. Santoro, S. V Roth and P. Müller-Buschbaum, *Adv. Energy Mater.*, 2016, **6**, 1600712.

31 B. R. Gautam, C. Lee, R. Younts, W. Lee, E. Danilov, B. J. Kim and K. Gundogdu, *ACS Appl. Mater. Interfaces*, 2015, **7**, 27586–27591.

32 T. Kim, R. Younts, W. Lee, S. Lee, K. Gundogdu and B. J. Kim, *J. Mater. Chem. A*, 2017, **5**, 22170–22179.

33 N. A. Pace, O. G. Reid and G. Rumbles, *ACS Energy Lett.*, 2018, **3**, 735–741.

34 J. T. Shieh, C. H. Liu, H. F. Meng, S. R. Tseng, Y. C. Chao and S. F. Horng, *J. Appl. Phys.*, 2010, **107**, 1–9.

35 T. Kirchartz, B. E. Pieters, J. Kirkpatrick, U. Rau and J. Nelson, 2011, **115209**, 1–13.

36 D. Bartesaghi, I. del C. Pérez, J. Kniepert, S. Roland, M. Turbiez, D. Neher and L. J. A. Koster, *Nat. Commun.*, 2015, **6**, 7083.

37 J. Schafferhans, A. Baumann, A. Wagenpfahl, C. Deibel and V. Dyakonov, *Org. Electron.*, 2010, **11**, 1693–1700.

38 Q. Dong, C. Hoi, Y. Ho, H. Yu, A. Salehi and F. So, , DOI:10.1021/acs.chemmater.9b01292.

39 B. A. Macleod, B. J. Tremolet De Villers, P. Schulz, P. F. Ndione, H. Kim, A. J. Giordano, K. Zhu, S. R. Marder, S. Graham, J. J. Berry, A. Kahn and D. C. Olson, *Energy Environ. Sci.*, 2015, **8**, 592–601.

40 X. Jiao, L. Ye and H. Ade, *Adv. Energy Mater.*, 2017, **7**, 1700084.

41 Y. Firdaus, V. M. Le Corre, J. I. Khan, Z. Kan, F. Laquai, P. M. Beaujuge and T. D. Anthopoulos, *Adv. Sci.*, 2019, **6**, 1802028.

42 J. A. Bartelt, D. Lam, T. M. Burke, S. M. Sweetnam and M. D. McGehee, *Adv. Energy Mater.*, 2015, **5**, 1500577.

43 W. Tress, M. Yavari, K. Domanski, P. Yadav, B. Niesen, J. P. Correa Baena, A. Hagfeldt and M. Graetzel, *Energy Environ. Sci.*, 2018, **11**, 151–165.

44 X. Du, T. Heumueller, W. Gruber, A. Classen, T. Unruh, N. Li and C. J. Brabec,

Joule, 2019, **3**, 215–226.

45 Q. Burlingame, X. Tong, J. Hankett, M. Slootsky, Z. Chen and S. R. Forrest, *Energy Environ. Sci.*, 2015, **8**, 1005–1010.

46 V. Savikhin, L. K. Jagadamma, L. J. Purvis, I. Robertson, S. D. Oosterhout, C. J. Douglas, I. D. W. Samuel and M. F. Toney, *iScience*, 2018, **2**, 182–192.